

# A study of a fixed trapezoidal section in regular waves using a generalized weak-scatterer model

**Tong, Chao; Shao, Yanlin; Bingham, Harry B.; W. Hanssen, Finn-Christian**

*Publication date:*
2022

*Document Version*
Publisher's PDF, also known as Version of record

# A study of a fixed trapezoidal section in regular waves using a generalized weak-scatterer model

Chao Tong[1], Yanlin Shao[1]*, Harry B. Bingham[1], Finn-Christian W. Hanssen[2]

1: Department of Mechanical Engineering, Technical University of Denmark, 2800 Lyngby, Denmark
2: NTNU AMOS, Department of Marine Technology, NTNU, Trondheim, Norway

## 1 Introduction

The original weak-scatterer (OWS) hypothesis, pioneered by Pawlowski [1], assumes a vertical displacement of the scattered wave elevation from the underlying incident wave, which leads to an inconsistency when the surface-piercing structure has flares near the waterline. Thus, the predicted waterline position using the superposition of the incident and scattered waves will separate from the surface of the structure, particularly for incident waves with large amplitudes and structures with large flare angles. With this in mind, we have re-derived the free-surface boundary conditions based on a generalized weak-scatterer (GWS) approximation to avoid this inconsistency. The basic idea of GWS is that the fully nonlinear (FN) free-surface conditions are linearized about the incident wave surface, but using a Taylor expansion along an arbitrary direction which can be manually prescribed in practice according to the geometry of the structure. In this way, we can precisely capture the waterline position on the structure at each time step of the solution. Accordingly, expressions for the wave loads acting on the structure based on direct pressure integration are also derived based on the same assumption.

## 2 Generalized weak-scatterer approximation

A Cartesian coordinate system $Oxz$ is defined with its origin located at the mean water level and the $Oz$ axis oriented positively upwards. For a surface-piercing structure with a large flare, like a wedge or a ship bow, it is reasonable to introduce a direction tangential to the structure's surface to track the waterline intersection. In this case, we assume that the total velocity potential and the free surface displacement $(\varphi, \mathbf{r})$ can be split into the incident component $(\varphi_I, \mathbf{r}_I)$ and the scattered component $(\varphi_S, \mathbf{r}_S)$, where $\mathbf{r}_I = (x_I, \eta_I)$ and $\mathbf{r}_S = (x_S, \eta_S)$:

$$\varphi = \varphi_I + \varphi_S, \qquad \mathbf{r} = \mathbf{r}_I + \mathbf{r}_S. \tag{1}$$

Same as in the OWS hypothesis, we introduce a small parameter $\epsilon$ to denote the smallness of the quantities associated with the scattered waves, and assume that $\varphi_S/\varphi_I \in O(\epsilon)$ and $r_i^S/r_i^I \in O(\epsilon), (i = 1, 2, 3)$, where $r_i^I$ and $r_i^S$ represent position components of $\mathbf{r}_I$ and $\mathbf{r}_S$, respectively.

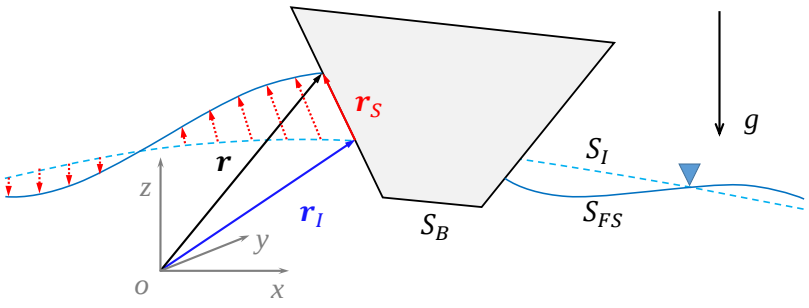


Figure 1: An illustration of wave-structure interaction problem within the frame of weak-scatterer approximation.

An arbitrary Lagrangian-Eulerian (ALE) approach is adopted to track the wave markers. On the instantaneous free surface, the kinematic and dynamic free-surface boundary conditions in the inertial reference frame are expressed as:

$$\frac{\delta \eta}{\delta t} = \frac{\partial \varphi}{\partial z} - (\nabla\varphi - \mathbf{V}) \cdot \nabla\eta, \qquad \frac{\delta \varphi}{\delta t} = -g\eta - \frac{1}{2}\nabla\varphi \cdot \nabla\varphi + \mathbf{V} \cdot \nabla\varphi. \tag{2}$$

Inserting (1) into (2), taking the Taylor series expansion of the free-surface boundary conditions from the incident wave along an arbitrary direction, and neglecting terms higher than the first order in $\epsilon$, finally we

*Corresponding author. E-mail addresses: yshao@mek.dtu.dk

obtain the free-surface boundary conditions for the scattered wave:

$$\frac{\delta\eta_S}{\delta t} = \frac{\partial\varphi_S}{\partial z} - (\nabla\varphi_I - \mathbf{V})\cdot\nabla\eta_S - \nabla\varphi_S\cdot\nabla\eta_I - \nabla\left(\frac{\partial\eta_I}{\partial t} - \frac{\partial\varphi_I}{\partial z} + \nabla\varphi_I\cdot\nabla\eta_I\right)\cdot\mathbf{r}_S \quad \text{at } \mathbf{r}=\mathbf{r_I}, \tag{3}$$

$$\frac{\delta\varphi_S}{\delta t} = -g\eta_S - (\nabla\varphi_I - \mathbf{V})\cdot\nabla\varphi_S - \nabla\left(\frac{\partial\varphi_I}{\partial t} + g\eta_I + \frac{1}{2}\nabla\varphi_I\cdot\nabla\varphi_I\right)\cdot\mathbf{r}_S \quad \text{at } \mathbf{r}=\mathbf{r_I}. \tag{4}$$

Here $\mathbf{V}$ is a prescribed velocity which is tangential to the boundary of the surface-piercing structure at the waterline, meaning that $\mathbf{V}$ and $\mathbf{r}_S$ are parallel to each other at the free-surface intersection. Away from the structure, the direction of $\mathbf{V}$ is gradually changed to purely vertical. The unit direction vector of $\mathbf{r}_S$ is defined as $\mathbf{l}_S = (l_1, l_2)$, and the vertical component of $\mathbf{V}$ is $V_2 = \partial\eta_I/\partial t + \mathbf{V}\cdot\nabla\eta_I$ for a fixed structure. The relation between $\mathbf{V}$ and $\mathbf{r}_S$ gives $\mathbf{V} = (l_1 V_2/l_2, V_2)$ straightforwardly.

For the Neumann boundaries, a no-flux condition normal to the structure surface should be satisfied on the instantaneous wetted body surface: $\partial\varphi_S/\partial n = -\partial\varphi_I/\partial n + \mathbf{V_b}\cdot\mathbf{n}$, while on the stationary seabed or tank walls: $\partial\varphi_S/\partial n = 0$. The governing equation for the scattered potential field is the Laplace equation $\nabla^2\varphi_S = 0$. Enclosed by the described mixed Dirichlet-Neumann boundaries, a BVP can be formulated and solved.

The instantaneous pressure on the structure surface can be computed from Bernoulli's equation:

$$P = -\rho(\varphi_t + \frac{1}{2}|\nabla\varphi|^2 + gz). \tag{5}$$

where $\rho$ is the fluid density. Therefore, the hydrodynamic forces $\mathbf{F}_{hydro} = (f_1, f_2, f_3)$ and moments $\mathbf{M}_{hydro} = (f_4, f_5, f_6)$ can subsequently be obtained by integrating the pressure over the structure's wetted surface. The integrals over the exact wetted body surface $S_{WB}$ are split into two parts: one is over the wetted body surface $S^I_{WB}$ below the intersection between the body and the incident wave, and the other is introduced because of the scattered wave:

$$f_i = -\iint_{S_{WB}} Pn_i\,\mathrm{d}s = -\iint_{S^I_{WB}} Pn_i\,\mathrm{d}s - \iint_{\Delta S} Pn_i\,\mathrm{d}s, \tag{6}$$

where $n_i$ are the six components of the generalized unit normal vector, $(n_1, n_2, n_3) = \mathbf{n}$, and $(n_4, n_5, n_6) = \mathbf{r}_b \times \mathbf{n}$. Here $\mathbf{n}$ points into the fluid. The second term due to the scattered waves can also be separated into two parts for convenience:

$$-\iint_{\Delta S} Pn_i\,\mathrm{d}s = \rho\iint_{\Delta S}\left(\varphi_t + \frac{1}{2}|\nabla\varphi|^2\right)n_i\,\mathrm{d}s + \rho\iint_{\Delta S} gzn_i\,\mathrm{d}s = \Pi_1 + \Pi_2. \tag{7}$$

Since the integrand of $\Pi_1$ is not a constant within the strip area $\Delta S$ but a function of $\mathbf{r}_S$, in order to obtain the integral, taking the Taylor expansion of the integrand at the incident wave position at the incident wave $\mathbf{r}_I$ yields

$$\begin{aligned}\Pi_1 =& \rho\iint_{\Delta S}\left(\left[\varphi_t + \frac{1}{2}[\nabla\varphi|^2\right]_{\text{at }\mathbf{r}_I} + \left[\nabla\left(\varphi_t + \frac{1}{2}|\nabla\varphi|^2\right)\cdot(\mathbf{r}-\mathbf{r}_I)\right]_{\text{at }\mathbf{r}_I} + O(\epsilon^2)\right)n_i\,\mathrm{d}s \\ \approx& \rho\oint_{\Gamma_I} r_S\left(\varphi_t + \frac{1}{2}|\nabla\varphi|^2\right)n_i\,\mathrm{d}\Gamma + \rho\oint_{\Gamma_I}\frac{1}{2}r_S^2\left[\nabla\left(\frac{\partial\varphi_I}{\partial t} + \frac{1}{2}\nabla\varphi_I\cdot\nabla\varphi_I\right)\cdot\mathbf{l}_S\right]n_i\,\mathrm{d}\Gamma,\end{aligned} \tag{8}$$

where $\Gamma_I$ indicates the waterline of the structure due to the incident wave. $r_S$ is the amplitude of $\mathbf{r}_S$ with the same sign as the vertical component of $\mathbf{r}_S$, and $\theta$ denotes the angle between the vector $\mathbf{r}_S$ and the $z$-axis in the inertial coordinate system so that $\eta_S = r_S\cos\theta$. As for the second integral $\Pi_2$,

$$\Pi_2 = \rho\iint_{\Delta S} gzn_i\,\mathrm{d}s = \rho\oint_{\Gamma_I}\int_0^{r_S} g(\eta_I + z_S)n_i\,\mathrm{d}r\mathrm{d}\Gamma = \rho\oint_{\Gamma_I}\frac{1}{2}g(2\eta_I r_S + r_S^2\cos\theta)n_i\,\mathrm{d}\Gamma. \tag{9}$$

The hydrodynamic loads on the structure can be finally assembled as

$$\begin{aligned}f_i =& \rho\iint_{S^I_{WB}}\left(\varphi_t + \frac{1}{2}|\nabla\varphi|^2 + gz\right)n_i\,\mathrm{d}s + \rho\oint_{\Gamma_I} r_S\left(\varphi_t + \frac{1}{2}|\nabla\varphi|^2 + g\eta_I\right)n_i\,\mathrm{d}\Gamma \\ &+\rho\oint_{\Gamma_I}\frac{1}{2}r_S^2\left[\nabla\left(\frac{\partial\varphi_I}{\partial t} + \frac{1}{2}\nabla\varphi_I\cdot\nabla\varphi_I\right)\cdot\mathbf{l_S} + g\cos\theta\right]n_i\,\mathrm{d}\Gamma.\end{aligned} \tag{10}$$

It can be observed that the magnitude for the main wetted body surface integral is of $O(1)$, for the first waterline integral is of $O(\epsilon)$ and for the second waterline integral is of $O(\epsilon^2)$, respectively.

## 3 Stability analysis

A fixed trapezoidal cylinder with large flare angle subject to an incident wave is considered. By observing the GWS free surface boundary conditions in Eqn.(3) and (4), it can be seen that there exist convective terms, which make the condition similar to that for a seakeeping problem for a ship with forward speed. When the forward speed becomes significant, instability may occur if an explicit time-integration scheme is applied without special treatment of the convective terms. Here, a linear matrix-based eigenvalue stability analysis is performed to understand the stability properties of the numerical algorithms. We consider the 2D linearized kinematic and dynamic GWS free-surface boundary conditions containing the $x$-convective terms in matrix form:

$$\frac{\delta}{\delta t}\begin{pmatrix}\eta_S\\ \tilde{\varphi}_S\end{pmatrix} = \begin{pmatrix}-U_x\frac{\partial}{\partial x} & \frac{\partial}{\partial z}\\ -g & -U_x\frac{\partial}{\partial x}\end{pmatrix}\begin{pmatrix}\eta_S\\ \tilde{\varphi}_S\end{pmatrix}, \tag{11}$$

where the convective velocity is defined as $U_x = \frac{\partial \varphi_I}{\partial x} - V_x$, $\eta_S$ is the scattered wave elevation, and $\tilde{\varphi}_S = \varphi_S(x, 0, t)$ is the scattered velocity potential at the mean water level. The space-discretized form of Eqn. (11) can be written as

$$\frac{\delta}{\delta t}\begin{pmatrix}\{\eta_S\}\\ \{\tilde{\varphi}_S\}\end{pmatrix} = \begin{pmatrix}[U][D_x^f] & [\Theta_z]\\ -g[I] & [U][\Theta_x]\end{pmatrix}\begin{pmatrix}\{\eta_S\}\\ \{\tilde{\varphi}_S\}\end{pmatrix} \Rightarrow \frac{\delta\{q\}}{\delta t} = [J]\{q\}. \tag{12}$$

Here $\{q\} = [\eta_{S,1}, \eta_{S,2}, \cdots, \eta_{S,N_m}, \tilde{\varphi}_{S,1}, \tilde{\varphi}_{S,2}, \cdots, \tilde{\varphi}_{S,N_m}]^{\mathrm{T}} = [\{\eta_S\}; \{\tilde{\varphi}_S\}]$, where $N_m$ is the number of wave markers. $[I]$ is an identity diagonal matrix, while $[U]$ is a diagonal matrix containing the convective velocities of the wave markers. The matrix operator $[D_x^f]$ differentiates $\eta_S$ with respect to $x$, whose non-zero elements are the weighting coefficients of a specific finite difference scheme. The global equation system is recalled

$$[A]\{\varphi_S\} = \{b\} \doteq [Q]\{\tilde{\varphi}_S\}, \tag{13}$$

where $[Q]$ is an operator matrix to distribute the free surface boundary conditions $\{\tilde{\varphi}_S\}$ into the corresponding positions of the global boundary value vector $\{b\}$. By doing this, after some simple manipulations, we can get expressions for $[\Theta_x]$ and $[\Theta_z]$:

$$[\Theta_x] = [D_x^c][A]^{-1}[Q], \quad [\Theta_z] = [D_z^c][A]^{-1}[Q], \tag{14}$$

in which $[D_x^c]$ and $[D_z^c]$ are operator matrices to take the $x$ and $z$ derivative of $\{\tilde{\varphi}_S\}$ at $z = 0$.

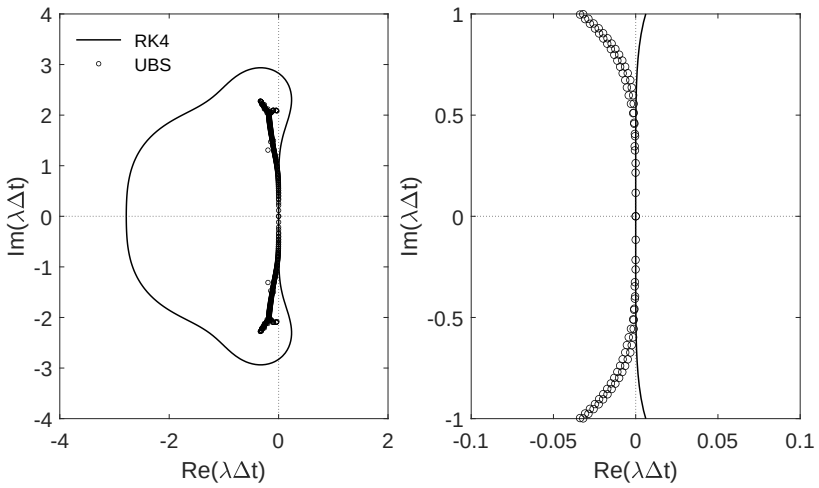


Figure 2: Eigenvalues of a $3^{rd}$-order upwind-biased scheme for the wave steepness $kH = 0.2$. Zoomed-in view near the origin is also displayed in the right plot.

For the discretization of the free-surface boundary conditions discussed above, the eigenvalues of the matrix $[J]$ can be computed numerically. To guarantee stability, all the eigenvalues of matrix $[J]$ multiplied by the time step $\Delta t$ must be inside the stability region for a given time stepping scheme. In our study, the $4^{th}$-order explicit Runge-Kutta (RK4) scheme is used.

There are two convective derivatives in both the dynamic and kinematic free-surface conditions, i.e. $\partial\varphi_S/\partial x$ and $\partial\eta_S/\partial x$, which are calculated by a $3^{rd}$-order upwind-biased scheme (UBS) to ensure stability. At Neumann boundaries, we require ghost nodes outside the fluid domain to calculate the convective derivatives. If upwind markers on the free surface can be found, then extrapolation is used; otherwise, a Neumann boundary condition is imposed to compute the values on the ghost points. Here a linearized Neumann

boundary condition is provided as reference:

$$\frac{\partial \eta_S}{\partial n} = \frac{1}{g}\frac{\partial}{\partial t}\left(\frac{\partial \varphi_I}{\partial n}\right). \tag{15}$$

In general, instability issues come mainly from the wave markers on the lee side of the structure, but the scheme is applied everywhere. The stability eigenvalues for the $3^{rd}$-order upwind-biased scheme (UBS) are shown in Fig. 2. It can be seen from the zoomed-in plot that all eigenvalues are inside the stability region of the RK4 scheme. More details of the stability analysis can be found in [3].

## 4 Numerical application

A fixed trapezoidal ship section with a flare angle $\theta = 30°$, semi-submerged in regular waves is studied here. The flare angle $\theta$ is defined as the angle between the side wall of the section and the vertical direction in the inertial coordinate system $Oxz$ that is located at the middle of the tank at the mean water level. The wave tank has a length $L = 8L_w$, the water depth is $h = L_w$, and the length of the damping zone is $L_{damp} = 2L_w$. The incident wavelength is set as $L_w = 2.5$ m in our simulations and the wave period is $T$. The wave height $H = 0.11$ m. The incident wave is generated by the stream function theory [2]. The bottom breadth of the trapezoidal section is $B = 0.2L_w$ and the draught is $d = 0.1L_w$.

A detailed demonstration of the dynamic fluid pressure distribution over the instantaneous wetted body surface, and the wave profile close to the waterline points for this fixed trapezoidal ship section in waves with $H = 0.11$ m is presented in Fig. 3. The snapshots represent different time instants during the $31^{st}$ wave period. Generally speaking, the consistency between the GWS and FN models [4] is deemed satisfactory and promising for both the wave elevation and the pressure distribution. Note that the pressure distribution of the GWS solutions in Fig. 3 results from the intersection between the incident wave and the structure, corresponding to the mean wetted body surface integral in Eqn. (10). The difference between the OWS and GWS can not be demonstrated here due to the lack of space and will be presented during the workshop.

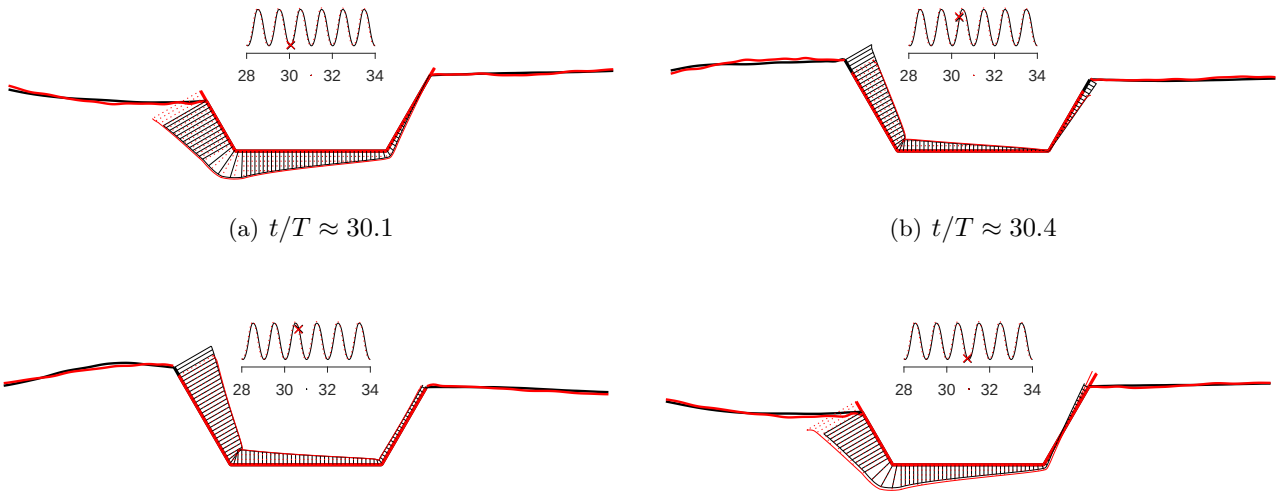


(a) $t/T \approx 30.1$ (b) $t/T \approx 30.4$

(c) $t/T \approx 30.7$ (d) $t/T \approx 31$

Figure 3: Dynamic pressure distribution and free surface elevation near waterline on the body at different time instants. The analysis of the GWS solutions (red) is compared with the FN solutions (black). The corresponding time instants are indicated with red and black cross in the time series of horizontal force.

## Acknowledgment

This work is funded by the Chinese Scholarship Council (No.201906230317) and the Department of Mechanical Engineering at Technical University of Denmark.

## References

[1] Pawlowski, J., 1994. A nonlinear theory of ship motion in waves .

[2] Rienecker, M., Fenton, J., 1981. A fourier approximation method for steady water waves. Journal of fluid mechanics 104, 119–37.

[3] Tong, C., Shao, Y., Bingham, H.B., Hanssen, F.C.W., . A generalized weak-scatterer approximation for nonlinear wave-structure interaction in marine hydrodynamics (submitted) .

[4] Tong, C., Shao, Y., Bingham, H.B., Hanssen, F.C.W., 2021. An adaptive harmonic polynomial cell method with immersed boundaries: Accuracy, stability, and applications. International Journal for Numerical Methods in Engineering 122, 2945–80.